

On the use of CFD to obtain head loss coefficients in hydraulic systems and its application to liquid metal MHD flows in nuclear fusion reactor blankets

Daniel Suarez *

Elisabet Mas de les Valls

Lluís Batet

* Corresponding author: daniel.suarez.cambra@upc.edu

Departament de Física, Universitat Politècnica de Catalunya, Barcelona, Spain

August 2021

Abstract

When an incompressible fluid flows through a contraction in a conduit, the increase in the kinetic energy of the fluid is accompanied by a pressure drop. This pressure drop is not to be assimilated with head loss. If downstream the fluid encounters an expansion in the conduit, the energy conversion will take place in the opposite way. Therefore, when a geometrical singularity is analysed to assess its contribution to the pumping power requirements of the system, the whole mechanical energy transfer of the fluid in the singularity has to be taken into account, and not only the pressure variation. The first part of the present work establishes a method to obtain head loss coefficients in geometric singularities of hydrodynamic circuits using the results of Computational Fluid Dynamics (CFD) calculations. These coefficients are of interest when modelling the whole system with a 1D system code, for instance. In the second part of the article, the method is applied to a more complex case, involving magnetohydrodynamic (MHD) phenomena. Thus, a prototypical channel singularity in a liquid metal circuit subject to a magnetic field is analysed. The layout is representative of a case that could be found in the liquid metal blankets to be used in nuclear fusion reactors. The influence of the MHD phenomena is studied and the differences with a purely hydrodynamic case are pointed out. The MHD analyses have been done in the Marconi High Performance Computing facility, using 48 cores, each case needing between one and two weeks to complete.

1. Introduction

Some of the breeding blanket designs proposed for DEMO contain liquid metal, which flows along the cooling channels of the blanket system. The induced MHD phenomena are well known when the channel is straight [1]. Although final designs are not yet ready, the blanket modules will likely feature expansions and contractions of the liquid metal conduits under the magnetic field. In these 3D MHD flows, axial electric currents will be induced and will contribute to increasing the head losses in the system; this will result in higher requirements for pumping power and structural strengths.

The influence of MHD induced pressure drop in breeding blanket liquid metal systems has been addressed in numerous prior works. Malang et al., in 1991 [2], showed results of preliminary studies regarding head losses in different geometries in the Dual Coolant Lead-Lithium (DCLL) design.

Molokov, in 1995 [3], discussed the dependence of the 3D head losses on the MHD characteristic dimensionless parameters such as the interaction parameter N and the Hartmann number M (as it is used there), depending on the flow regime for manifolds where expansions can be found.

Müller and Bühler, in 2001 [1], derived mathematically the regime thresholds regarding the dimensionless parameters for 2D expansions in the direction of the external magnetic field.

Mistrangelo and Bühler, in 2007 [4], numerically studied in detail the flow topology and the pressure drop associated with rectangular channel expansions in the direction of the magnetic field.

Bühler et al., in 2007 [5], completed the analysis in the MEKKA laboratory, showing great accuracy of the theoretical pressure gradient along the expansion with the experimental results.

Smolentsev et al., in 2018 [6], analyzed the Dual-Coolant Lead-Lithium (DCLL) blanket for the Fusion Nuclear Science Facility (FNSF). Authors highlighted that the contribution of the 3D MHD effects to the pressure drop in the blanket cannot be avoided, even with channel insulators like Flow Channel Inserts, because they are caused by axial electric currents generated in the fluid. For insulated channels, locations of highest contribution to pressure drop are the access pipes (in the fringing magnetic field), and the 3D expansions and manifold distributors into the blanket channels.

Tassone et al., in 2020 [7], published a detailed analysis of the influence of the piping assembly on the overall pressure drop of the liquid metal flow in the Water Cooled Lead-Lithium (WCLL) blanket.

Smolentsev et al., in 2021 [8], reviewed the liquid metal MHD related pressure drop problem, ranging from theoretical background to practical examples.

Previous works done by the authors [9] over DCLL blanket manifold geometries where multiple outlets were considered concluded that, in those cases where outflow area is greater than inflow area, the flow could experience a pressure gain instead of a

pressure drop. This revealed that the use of the *pressure drop* concept for calculating the mechanical energy loss in the domain was inadequate. Instead, the use of the *head loss* concept seemed more adequate. The analyses used the energy conservation equation (from which Bernoulli's equation, often used in incompressible hydraulic systems design, can be derived) and concluded in the development of a calculation tool for the mechanical energy loss (head loss, or momentum transfer) based on the mechanical energy balance between the inlet and outlet boundaries, regardless of the phenomena occurring within the domain.

The first part of this work (Section 2) is devoted to the description of the method, and the validation of the calculation procedure. The theoretical approach to the development of the tool is outlined in subsection 2.1. This approach allows to model the 3D result of a CFD simulation as a 0D result, such as the dimensionless head loss coefficient. The result is of great interest for system code modelling. For example, it could help in assessing the head losses in a DCLL manifold such as that proposed by Khodak et al. [10] or in a WCLL such as that proposed by Tassone et al. [7].

The calculation tool has been validated (subsection 2.2) with hydrodynamic laminar contraction cases found in literature (Astarita and Greco [11], and Kaye and Rosen [12]). A hydrodynamic laminar expansion case has been used to test the soundness of the approach (subsection 2.3).

In the second part of this work (Section 3), the calculation procedure is applied to MHD expansions and contractions with conducting walls. In the cases studied, the appearance of different M-shaped profiles associated to different Hartmann numbers (Ha) at inlet and outlet varies the velocity distribution in the fully developed profile, i.e. the α kinetic energy correction factor. The influence of the variation of α (along with other parameters) in the head loss is analyzed in Section 4. Finally, some conclusions are drawn (Section 5).

The tool has been implemented in OpenFOAM, the toolkit used for the calculation of the aforementioned systems. Since the calculation of 3D MHD flows requires high computational resources, the simulations were performed in *Marconi HPC*.

2. Description and validation of the proposed method to retrieve the head loss coefficient

2.1. Theoretical background

In the constructive design phase of a hydraulic system, head loss calculations in pipes and components are an important part of the engineering analysis. The result of such calculations may be used, for instance, to size a pump or fan, or to identify singular components where head losses exceed the acceptable limits. Since a wide range of geometries can be encountered when treating internal flows passing through pipes, engineers rely on laboratory experimental data that provide correlations for head loss coefficients. These data are commonly collected in hydraulic handbooks where different

geometries and roughnesses are considered for flows at different regimes. Some very well-known examples of such handbooks are Idelchik [13], Brater [14], Miller [15] or CRANE [16].

One can find, in such references, that head loss is treated as a portion of the kinetic energy head that the fluid has lost, or transferred to internal energy, in the form of:

$$h_L = K_h \cdot \frac{U^2}{2g} \text{ in units of [m]} \quad (1)$$

$$h_L = K_h \cdot \rho \cdot \frac{U^2}{2} \text{ in units of [Pa]} \quad (2)$$

being U the flow characteristic velocity (so that $\dot{V} = U \cdot A$, where \dot{V} is the volumetric flow rate and A is the cross-sectional area), ρ the fluid density, and K_h the dimensionless head loss coefficient obtained from experimental results.

The straight pipes of a system and its geometric singularities are treated in a different manner. On the one hand, geometric singularities get a value of K_h depending of the flow regime (the Reynolds number, for example) and some geometry ratios, and are called minor losses. On the other hand, head losses by friction in straight pipes are called major losses and are treated using the Darcy's friction factor, f , multiplied by the dimensionless length, L/D , of the straight pipe. This has the form of:

$$h_L = \left(f \cdot \frac{L}{D}\right) \cdot \rho \cdot \frac{U^2}{2} \text{ in units of [Pa]} \quad (3)$$

where the terms within the brackets substitute the head loss coefficient (K_h) in the previous form, L is the pipe length and D is the pipe diameter.

Bernoulli theorem is frequently used in the analysis of hydraulic systems with an incompressible fluid:

$$E = \rho \cdot g \cdot z + p + \frac{\rho \cdot U^2}{2} = \text{constant} \quad (4)$$

in units of [Pa] or [J/m³].

In the expression above (Eq. 4), three terms are identified as contributors to the mechanical energy of the fluid. The first term is the elevation of the fluid (potential energy), the second term is the static pressure, and the last term is the kinetic energy per unit volume (dynamic pressure). E corresponds to the mechanical energy of a fluid particle and, unless there is some sort of energy transfer to a different kind of energy (e.g. internal energy), it remains constant, what means that, ideally, expansions or contractions can modify velocity and pressure but not E .

When using such a powerful tool as Bernoulli's equation one should consider its fundamental assumptions [17]:

- (i) the flow is steady,
- (ii) the flow is frictionless,
- (iii) there is no shaft work involved,

- (iv) the flow is incompressible,
- (v) there is no heat transfer involved,
- (vi) the flow goes along a streamline parallel to the pipe walls.

In order to correct the deviations that the second assumption may induce in the calculations, the head loss concept is introduced in the model. These energy losses when a fluid is passing from a point A to a point B in a system, are expressed as:

$$E_A = E_B + \sum_{i=0}^n h_{Li} \quad (5)$$

where n represents the number of singular mechanical energy sinks to consider, that can be straight pipes or geometric singularities, and h_{Li} is the head loss in a singularity or in a straight pipe segment i .

Further, the assumption of a fluid in a pipe being represented by a streamline of a velocity that corresponds to the flow rate through the section (U) is again an approximation. This approximation may lead to consider that the kinetic energy of the fluid at certain point of the system is represented by $\rho \cdot U^2/2$. This is, however, a wrong conclusion, since the velocity profile is not uniform over the cross-section of the conduit.

The error associated to this approximation can be addressed by considering the kinetic energy correction factor:

$$\alpha = \frac{KE_{actual}}{KE_{average}} = \frac{1}{A} \cdot \int \left(\frac{v(r)}{U} \right)^3 \cdot dA \quad (6)$$

where KE stands for kinetic energy, and $v(r)$ is the velocity encountered at the radius r of a round pipe section. This α kinetic energy correction factor must be applied to the Bernoulli approximation such that:

$$E_1 - E_2 = \left(\rho g z_1 + p_1 + \alpha_1 \cdot \frac{\rho \cdot U_1^2}{2} \right) - \left(\rho g z_2 + p_2 + \alpha_2 \cdot \frac{\rho \cdot U_2^2}{2} \right) = \sum_{i=0}^N h_{Li} \quad (7)$$

The application of the Bernoulli model in a piping network requires to use the proper α value. It is, however, very common to use $\alpha = 1$, ignoring the influence of the velocity distribution in the energy balance. In those flows showing a turbulent regime, α will get values fairly close to 1, usually 1.04 [13]. Therefore, in turbulent flows, the error associated with using the coefficient $\alpha = 1$ is rather small. When flows show a laminar regime, α can have values around 2, which can induce large calculation errors if not properly considered.

In contractions (or nozzles) or expansions (or diffusers), Eq. 7 illustrates that the mechanical energy lost at that point is not strictly the static pressure difference measured between the outlet and the inlet, considering the flow rate has to be maintained, i.e. $\dot{V} = U_1 \cdot A_1 = U_2 \cdot A_2$. In these cases, the formation of eddies in

counter-pressure flows like diffusers or sharp edges in nozzles can violate again the streamline assumption. However, engineers make use of this expression to perform a 0D mechanical energy balance of the system.

Bernoulli's equation might be derived from the momentum equation (Newton's second law) or from the energy conservation equation within a domain. The energy conservation equation possesses the required information to make the desired analysis. The steady form of this equation (in units of [W]) applied to a given open volume takes the form:

$$\dot{Q}_{net} + \dot{W}_{net} = \sum_{o=1}^{n_{outlet}} \dot{V}_o \cdot \rho \cdot \left(gz_o + h_o + \frac{U_o^2}{2} \right) - \sum_{i=1}^{n_{inlet}} \dot{V}_i \cdot \rho \cdot \left(gz_i + h_i + \frac{U_i^2}{2} \right) \quad (8)$$

where h is the specific enthalpy $h = u + p/\rho$, being u the specific internal energy. U corresponds to velocity perpendicular to the boundary cell faces.

The left hand side of Eq. 8 stands for the net rate of energy transfer (addition) to a control volume by heat (\dot{Q}_{net}) and work (\dot{W}_{net}). The right hand side stands for the difference between the rates of outgoing and incoming energy. In the CFD analyses that follow, these energy flows are evaluated at the n_{inlet} and n_{outlet} cell faces on the domain boundaries.

When considering incompressible flows, a simplification can be made without loss of generality in the analyses that follow below: the gravity term can be excluded of the Eq. 8, as it is always balanced with a component of the pressure that corresponds to gravity. Indeed, in a gravitationless system the method proposed will yield the same values for the head loss coefficient as when considering gravity, and, in the latter case, results will be the same in a horizontal conduit than in a vertical one.

Then, in a domain without external addition of heat nor work, Eq. 8 can be simplified in the form of Eq. 9, that equates the mechanical energy loss (\dot{P}_{loss}) to internal energy increase in the domain:

$$\dot{P}_{loss} = \dot{V} \cdot h_{L \text{ domain}} = \sum_{i=1}^{n_{inlet}} \dot{V}_i \cdot \left(p_i + \frac{\rho \cdot U_i^2}{2} \right) - \sum_{o=1}^{n_{outlet}} \dot{V}_o \cdot \left(p_o + \frac{\rho \cdot U_o^2}{2} \right) \quad (9)$$

where $h_{L \text{ domain}} = \rho \cdot \left(\sum_{o=1}^{n_{outlet}} u_o - \sum_{i=1}^{n_{inlet}} u_i \right)$ stands here as the head loss in the domain in units of [Pa] or [J/m³]. Please also note that $\dot{V} = \sum_{i=1}^{n_{inlet}} \dot{V}_i = \sum_{o=1}^{n_{outlet}} \dot{V}_o$. With this calculation, $h_{L \text{ domain}}$ is obtained and can be equaled to:

$$h_{L \text{ domain}} = h_{L \text{ inlet}} + h_{L \text{ singularity}} + h_{L \text{ outlet}} \quad (10)$$

where $h_{L \text{ inlet}}$ and $h_{L \text{ outlet}}$ are head losses associated with the friction of an equivalent upstream and downstream fully developed flows. The term $h_{L \text{ singularity}}$ contains, therefore, not only the energy loss associated to the geometry singularity region alone,

but also the energy loss associated to the reestablishment of a fully developed flow profile downstream and the influences upstream.

It is worth mentioning that the energy conservation equation is not the only method to compute the momentum transfer in CFD. The Second Law Analyses (SLA) [18], an alternative method based on the calculation of the entropy generation within the control volumes, has also shown good results [19].

Although the analysis focused on the pressure drop gives very interesting information regarding the local design requirements, the pumping specifications are retrieved from the overall energy balance of the system. The sum of the head losses in all the components of the system times the flow rate must not exceed the pumping capacity. The overall energy balance considers that the head losses in all the components of the system must match the pumping capacity. It is therefore very useful to obtain the value of this parameter for each component of the system by means of the energy balance.

In this work, the calculation of such energy balance in the volumetric domain computed with CFD has been coded. The following sections describe the application of the tool in sudden contractions and expansions of a circular pipe.

2.2. Code validation in a sudden contraction

The literature research on fundamental sudden contractions phenomena for laminar hydrodynamic flows revealed previous studies performed by Astarita et al. [11], Sylvester et al. [20], Kaye et al. [12], Durst et al. [21], and Bullen et al. [22]. As a first approach, contractions were preferred over expansions, since the larger recirculation zone produced in the latter makes the analysis more difficult. All the studies were performed in circular pipes. Kaye and Rosen's work [12] is especially interesting because it is very concise and finds out the interesting parameters for several contraction ratios. A very interesting and useful reference for the CFD modelling of the case is the study done by Ludicelo [23].

The validation case is a circular pipe contraction with a contraction ratio $\beta = D_{out}/D_{in} = 0.394\text{m}/0.989\text{m} = 0.4$. Using the symmetric condition, only one cell is considered in the angular direction. The studied cell has an opening angle of 2 degrees. The entrance region is mapped from a previously calculated fully developed case and considers 5 meters before the contraction. The exit region is 50 meters long to let the flow to develop fully. The inlet and outlet sections contain 150 and 60 cells in the radial direction, respectively. In the axial direction, the minimum cell size is 1/3 of the cell size in the radial direction with the smallest being right at the singularity. The cell to cell ratio towards the inlet is 1.02 and the ratio towards the outlet is 1.01. The mesh described here resulted in $\sim 65k$ cells, and is the coarsest mesh used in this study. The medium and fine meshes have $\sim 131k$ and $\sim 263k$ cells respectively. A mesh convergence study of the three meshes will be detailed below.

Figure 1 roughly shows the coarse mesh used near the singularity. The long inlet

and outlet are not shown, otherwise the singularity could not be appreciated.

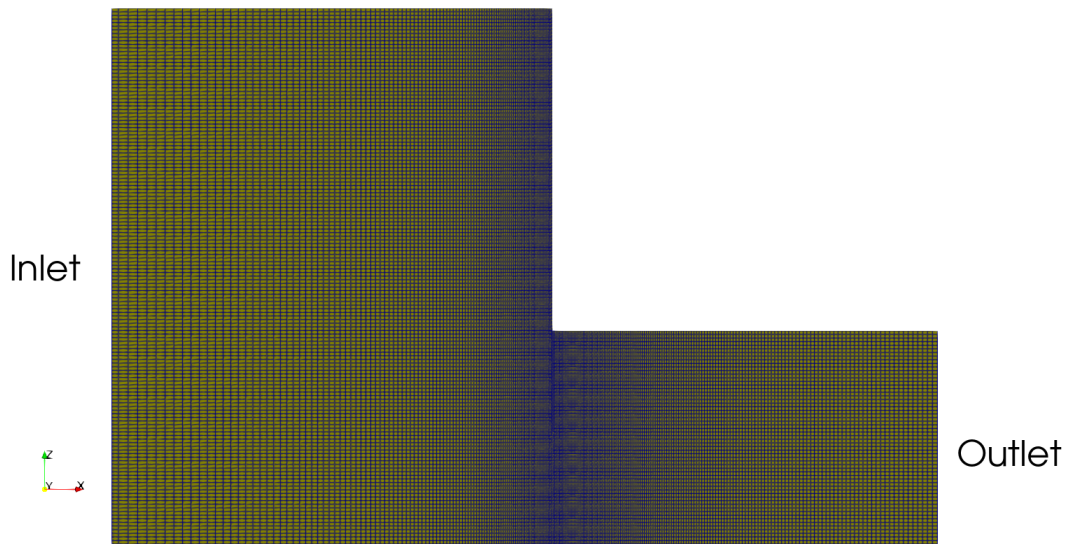


Figure 1. Mesh at the singularity

The velocity profile at the inlet patch is fixed and corresponds to that of the Poiseuille flow. At the outlet patch, the Neumann boundary condition (zero gradient) for the velocity field has been applied. The no-slip condition has been imposed at the walls. The pressure field is set to zero at the outlet patch and zero gradient at the inlet and at the walls. Selected discretization schemes have been central differencing scheme except for the advective term for which *Gauss linearUpwind* has been selected. No turbulence modelling is needed for this case since the flow remains laminar at the studied Reynolds numbers. The Reynolds number has been defined as: $Re = U_o \cdot D/\nu$, where U corresponds to the outlet characteristic velocity, D is the outlet pipe diameter, $\nu = \mu/\rho = 1e - 3$ is the kinematic viscosity for this case and μ is the dynamic viscosity. The cases studied were solved smoothly, showing oscillatory convergence. The velocity profile for the case with $Re=900$ is represented in Figure 2.

The calculations were performed following the well-known SIMPLE algorithm for incompressible fluids, originally developed by Patankar [24], and implemented as a solver in OpenFOAM® distribution [25] as *simpleFOAM*. The simulations were run in parallel using one core for every 10 thousand cells approximately. An algorithm was prepared to run a set of 110 simulations varying the Reynolds number at each of them, in order to obtain a tendency on the pressure drop and head loss associated with the sudden contraction.

The expected results for the pressure drop were those found in Astarita and Greco's [11] (Figure 3), although Kaye and Rosen [12] argued they were too high.

In Figure 3, U corresponds to the outlet mean velocity and K and K' in the figure correspond to the Hagenbach and Couette's coefficients that model the pressure drop found in a sudden contraction. In the present work, for the sake of consistency, these

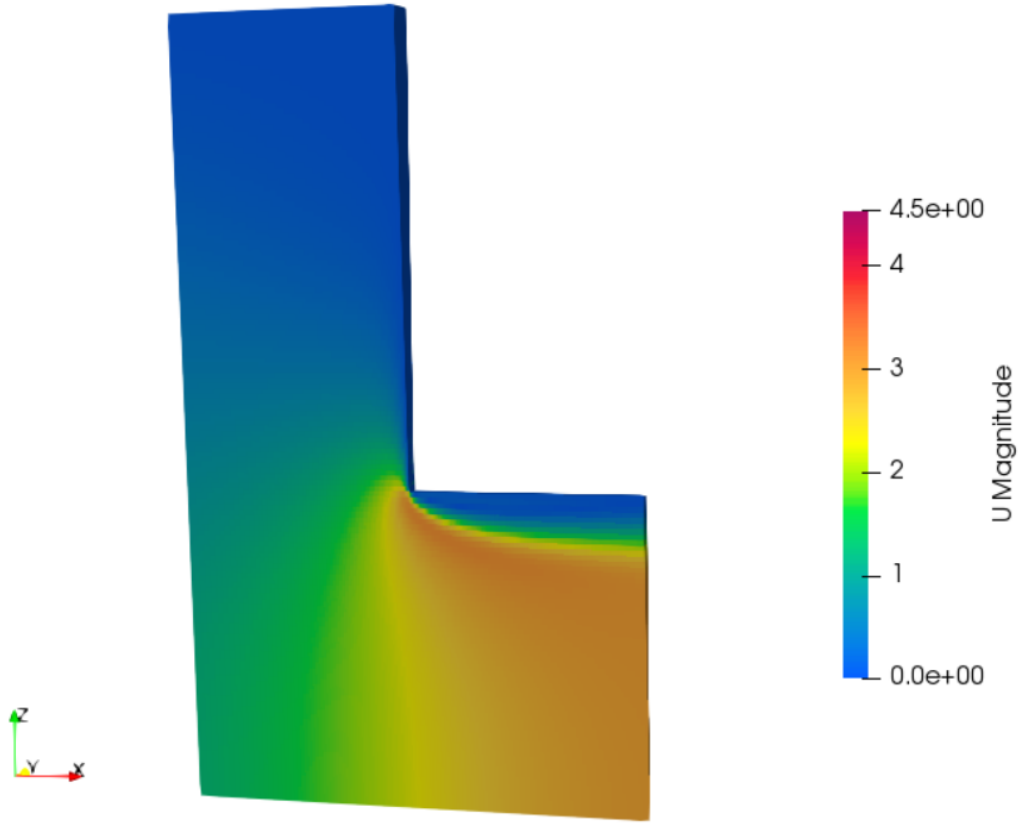


Figure 2. Velocity magnitude at the singularity for Re=900

two coefficients have been renamed as k_- and k'_- respectively, in order to keep K as the pressure drop coefficient. They are defined as:

$$K = \frac{\Delta p}{\rho U_0^2 / 2} = k_- + \frac{k'_-}{Re} \quad (11)$$

with k_- and k'_- coefficients that are function of β , as Kaye and Rosen [12] state:

$$k_- = 2.32 \pm 0.05 \cdot (1 - \beta^2) \quad (12)$$

$$k'_- = 159 \pm 30 \cdot (1 - \beta^2) \quad (13)$$

In Figure 4, the function proposed by Kaye and Rosen is plotted in solid blue, with coefficients $k_- = 2.37 \cdot (1 - \beta^2)$ and $k'_- = 129 \cdot (1 - \beta^2)$.

The values plotted in Figure 4 are discussed in the following paragraphs.

The results of K obtained in the simulations using the three meshes have been extrapolated using the Grid Convergence Index (GCI) algorithm (as described in Celik et al.[26]). These extrapolated values are represented by orange dots in Figure 4 and correspond to the actual results free of discretization errors. A function of the same form of Kaye and Rosen’s has been used to correlated them. This function uses the

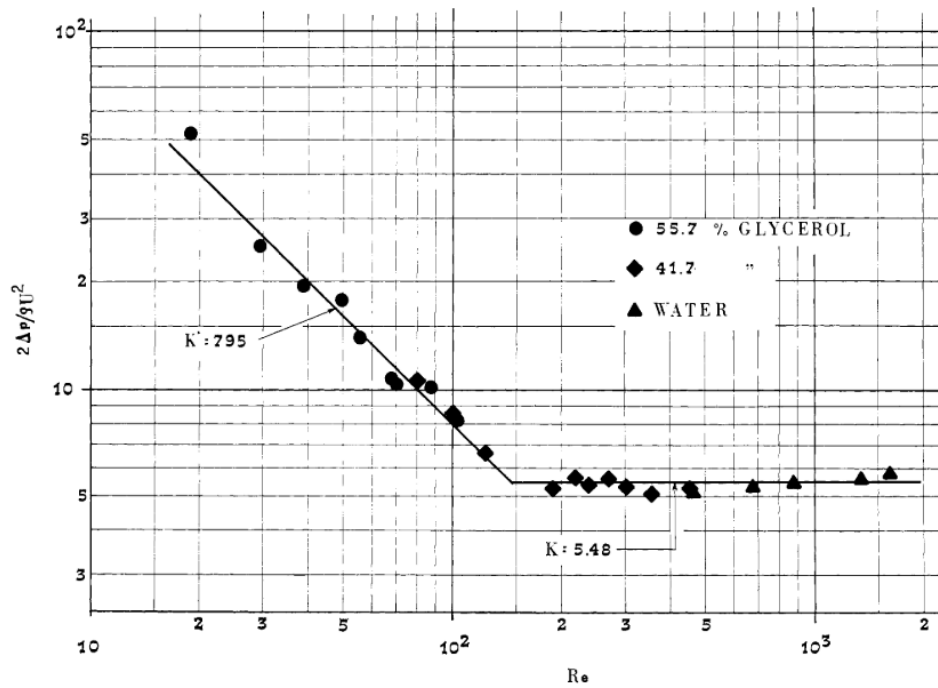


Figure 3. Data on excess pressure drop as for [11] for a contraction of $\beta = 0.4$. $k_- = 5.48$ and $k'_- = 795$

coefficients $k_- = 2.60 \cdot (1 - \beta^2)$ and $k'_- = 45 \cdot (1 - \beta^2)$, and is represented by a dotted green line. The results obtained confirm the accuracy of the simulations, although there are clear deviations compared to those of Kaye and Rosen for low Reynolds numbers.

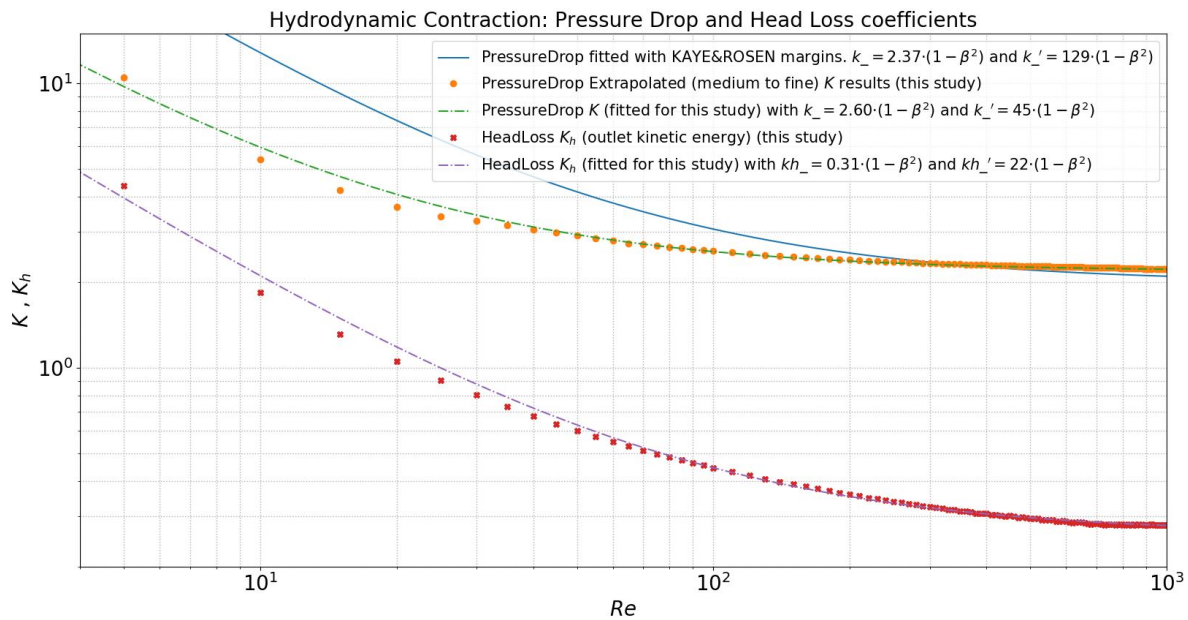


Figure 4. Pressure drop and head loss coefficients for laminar flow through a sudden contraction for different Re numbers

The GCI analysis has been conducted using a safety factor of 1.25 for each

simulation. Three meshes have been used, coarse (3), medium (2) and fine (1). Asymptotic range in the GCI analysis has not been fully obtained. The results of the GCI for the case of $Re = 700$ can be observed in Table 1. In the table, N_i represent the number of cells in each mesh, r is the ratio of the characteristic cell length between meshes (r_{32} from coarsest to medium and r_{21} from medium to fine), ψ is the parameter of interest (in this case k_-'), p is the apparent order of the discretization (related to the truncation error) and GCI is the error margin of the resulting value ψ_{ext}^{21} , which is the extrapolated result. e_a^{21} is the approximate relative error and e_{ext}^{21} is the relative error of the finest mesh versus the extrapolated result. The very low GCI value ($\sim 0.19\%$) indicates that the results are reliable and independent of the grid.

It can be seen in Figure 4 that there is a substantial difference between the line fitted for this study (dotted green) and the fit using the values proposed by Kaye and Rosen (solid blue). The former shows a very good agreement with the calculated data (the fit is almost coincident with data for Reynolds above 50). The latter (whose parameters were obtained experimentally) shows a large deviation with the calculated data for Reynolds values below 200. The causes for such deviation are unknown, although they could be caused by too low values of pressure drop and instrument errors in such narrow ranges. It is interesting to note too that this study was performed around fifty years ago and there were important differences between similar studies results, for example with Astarita and Greco's study [11].

The red crosses in Figure 4 represent the head loss coefficients for different Reynolds number, using the mean outlet kinetic energy. It is defined in Eqn. 14.

$$K_h = \frac{h_{L \text{ contraction}}}{\rho U_o^2 / 2} = kh_- + \frac{kh_-'}{Re} \quad (14)$$

A function of the same shape as Kaye and Rosen's has been used to correlate the head loss coefficients for different Reynolds numbers, as shown in Eqn. 14. The obtained values for the coefficients have been $kh_- = 0.31 \cdot (1 - \beta^2)$ and $kh_-' = 22 \cdot (1 - \beta^2)$ and are represented in Figure 4 by a dotted violet line.

The parameter K_h allows to easily calculate the mechanical energy loss in the contraction. The figure shows that the pressure drop is about one order of magnitude higher than the head loss; so, around 90% of the mechanical energy in form of pressure at the inlet is properly converted into kinetic energy in the outlet, while around 10% is lost by friction (irreversibilities) in the process.

The energy transformation within the geometric singularity can be easily understood rearranging Equation 7 to properly express the terms "pressure drop" (first term), "kinetic energy drop" (second term), equalling the "head loss" as expressed in Equation 15. Note that the gravity term has been omitted.

$$(p_1 - p_2) + \left(\alpha_1 \frac{\rho \cdot U_1^2}{2} - \alpha_2 \frac{\rho \cdot U_2^2}{2} \right) = h_{L \text{ singularity}} \quad (15)$$

The mechanical energy transformation for the case of $Re=1000$ is plotted in Figure

5. The magnitudes have been normalized dividing all three values by the head loss magnitude. The third column is therefore of magnitude 1.

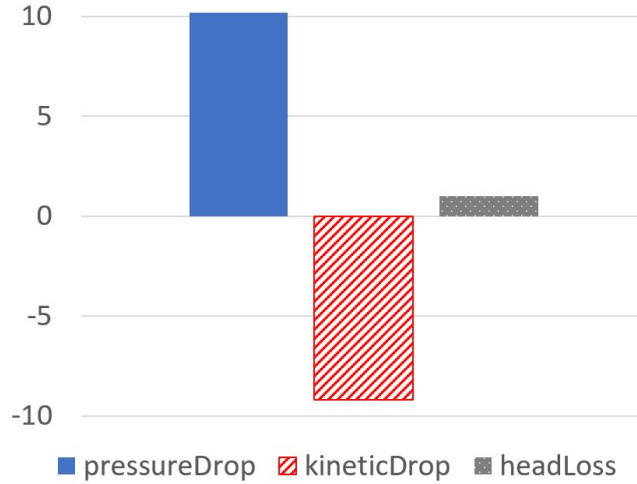


Figure 5. Energy transformation in a hydrodynamic contraction case ($Re=1000$). Pressure drop increases kinetic energy (negative kinetic energy drop) with around 10% of head lost

Table 1. Results of GCI analysis for K for $Re = 700$

$\psi = K$ for $Re = 700$	
Parameter	Value
N_3	~65 k
N_2	~131 k
N_1	~263 k
r_{32}	1.41
r_{21}	1.41
ψ_3	2.2607
ψ_2	2.2630
ψ_1	2.2562
p	3.13
ψ_{ext}^{21}	2.2527
e_a^{21}	0.0030
e_{ext}^{21}	0.0015
GCI_{fine}^{21}	0.19%

2.3. Application to a sudden expansion

The same procedure has been applied to a hydrodynamic sudden expansion with the same numerical details and geometry, but with the flow in the opposite direction. The results are shown in Figure 6.

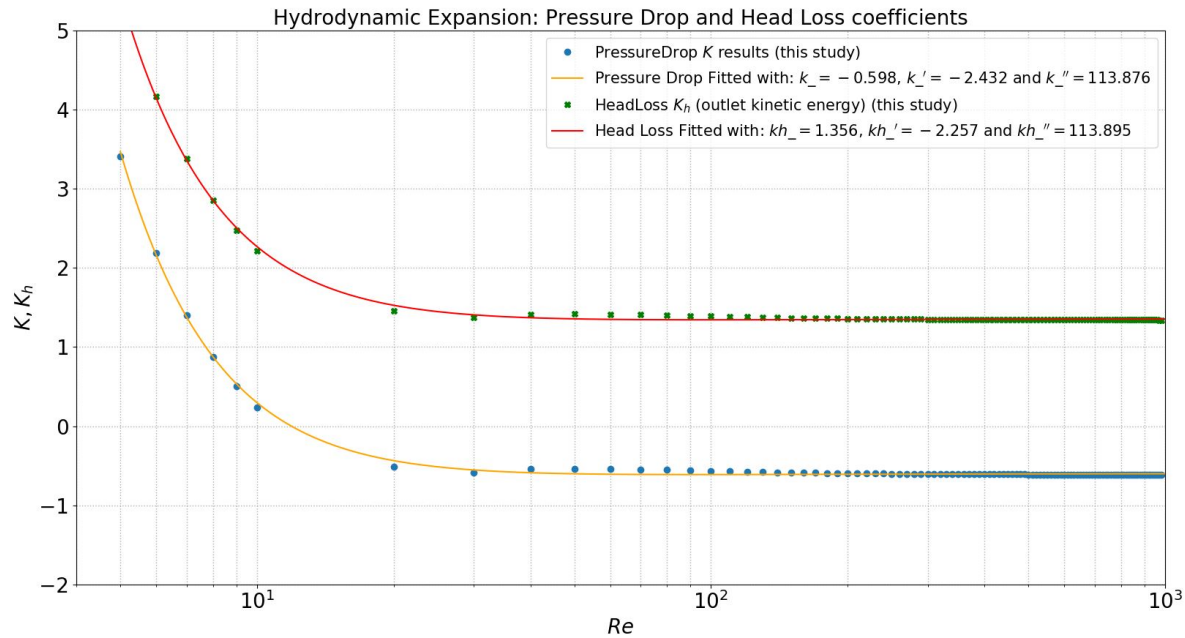


Figure 6. Pressure drop and head loss coefficients for laminar flow through a sudden expansion for different Re numbers

In this case the Reynolds is calculated using the inlet mean velocity and the inlet diameter. Figure 6 shows clearly that for Reynolds higher than 10 the K value is negative, which means that the outlet pressure is higher than the inlet pressure. Part of the kinetic energy of the inlet flow is transformed in pressure; therefore, the pressure drop is not a drop anymore, but a pressure gain.

In this figure, the usefulness of the head loss approach is very clear: it allows to compute and assign a mechanical energy loss to a geometric singularity in the hydraulic system. It can be seen that the pressure drop should not be confused with the head loss in Bernoulli's balance, since it can induce calculation errors.

Fitting curves have been adjusted to the calculated values of K and K_h . The curves and respective expressions are shown in Figure 6, superposed to the calculated K and K_h values. For a hydrodynamic expansion, the form of the fitted curves is different from that in Eq. 11 and Eq. 14. In this case, it has been found (this work) that the best fit is obtained adding a new term, with the Re number squared, as can be seen in the following expressions. Eq. 16 shows the relationship between Reynolds number and the pressure drop coefficient, and Eq. 17 relates Re with the head loss coefficient. The range of validity of the fitted curve is for Re between 5 and 1000. The coefficients in the case of the hydrodynamic expansion have not been related to the parameter β ,

since only the case of $\beta = 0.4$ has been studied.

$$K = \frac{\Delta p}{\rho U_0^2/2} = k_- + \frac{k_-'}{Re} + \frac{k_-''}{Re^2} \quad (16)$$

$$K_h = \frac{h_{L \text{ contraction}}}{\rho U_0^2/2} = kh_- + \frac{kh_-'}{Re} + \frac{kh_-''}{Re^2} \quad (17)$$

In the case of a hydrodynamic expansion, the mechanical energy transformation is plotted in Figure 7. The magnitudes have been normalized dividing all values by the head loss.

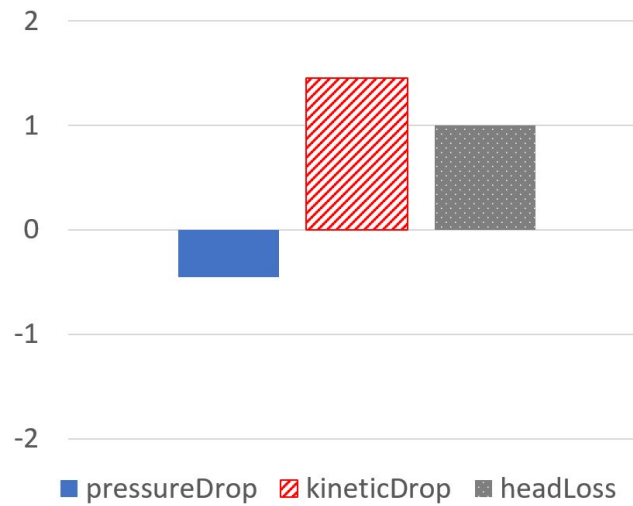


Figure 7. Energy transformation in a hydrodynamic expansion case ($Re=1000$). Pressure drop is negative (pressure increases) while kinetic energy drops

3. Application of the procedure for calculating the head loss coefficient to sudden expansions and contractions of liquid metal MHD flows

3.1. Related works

Assuming a rectangular channel with a magnetic field perpendicular to the flow, two simplified cases can be analysed: expansions can be in the direction of the magnetic field or perpendicular to the magnetic field.

The expansions perpendicular to the magnetic field direction enhance the formation of vortical structures that are allowed to keep rotating as far as the rotation axis is in the direction of the magnetic field until viscosity suppresses them.

An expansion in the direction of the magnetic field involves a modification of the Hartmann number and the wall conductivity ratio due to the change in geometry (the characteristic length used to define the liquid metal MHD flows in channels is half width of the channel in the direction of the magnetic field). This situation generates a difference in the electric potential in the flow direction, which will contribute to increase

the 3D electric current density. The 3D currents provoke additional Lorentz forces that oppose the flow, which will help to increase the head losses at the singularity.

Mistrangelo and Bühler [4], in 2007 at KIT, described in detail the main characteristics of the MHD flow in a sudden expansion in the direction of the magnetic field using the Theory of the Critical Points. Bühler et al. [5], in 2007, experimentally confirmed the theoretical predictions. The analysis carried out by Mistrangelo and Bühler in [4] included results from CFD using the finite volume method and results from the asymptotic approach for very high Hartmann numbers.

Recently, in 2018 a work performed by Smolentsev et al. [6], described the 3D pressure drops as large contributors to the overall system pressure drop. This work uses the following expression, well accepted by the fusion community:

$$\Delta p_{3D} = \xi \frac{\rho U^2}{2} \quad (18)$$

with $\xi = kN$, where k is found experimentally and is suggested to be $0.25 < k < 2$, and $N = Ha^2/Re$ is the interaction parameter. This approach is based on empirical results and is useful to estimate the order of magnitude; however, it lacks any theoretical background, in the authors' words. Müller and Bühler [1], in 2001 described theoretically the scaling of the expansion pressure drop in the magnetic field direction using a 2D model. Their work shows that the pressure drop scales differently depending on the ratio $Ha^{3/2}/N$.

3.2. Case description and numerical strategy

The MHD phenomena in sudden expansions have been studied in this work using the well validated in-house code developed by Mas de les Valls and described in [27] and based on the approach suggested by Ni et al. in 2007 [28]. The code has been written over OpenFOAM® and solves the MHD equations focused on the electric potential as main electric variable. The induced electric current density is then calculated and eventually a Lorentz force explicit term is included in the momentum equation. The momentum pressure-velocity coupling is solved using the PISO approach for incompressible flows. The discretization schemes have been central difference for all variables.

The code can solve the multi-material coupling, allowing to calculate the electric variables in the walls surrounding the channel. External walls are electrically insulated, thus, the electric potential field has zero gradient boundary condition. The electric potential extends throughout all the domain, i.e. the wall and the fluid regions are electrically coupled guaranteeing the conservation of normal current and electric potential at the solid/fluid interface.

The studied domain is a rectangular channel of dimensions 0.20 m x 0.10 m and 0.50 m long that encounters a sudden expansion and transforms the channel into a squared one with a cross section of 0.20 m x 0.20 m. The studied outlet length is 0.50 m. The expansion happens in the direction of the magnetic field. The surrounding

wall width is 1 mm. The domain has been halved using the symmetric condition of the flow. The dimensions are presented in Figures 8 and 9. The surrounding wall is represented in red and is made of EUROFER material while the flowing fluid is lead-lithium eutectic represented in grey. The physical properties of the PbLi are retrieved from [29] at 400°C.

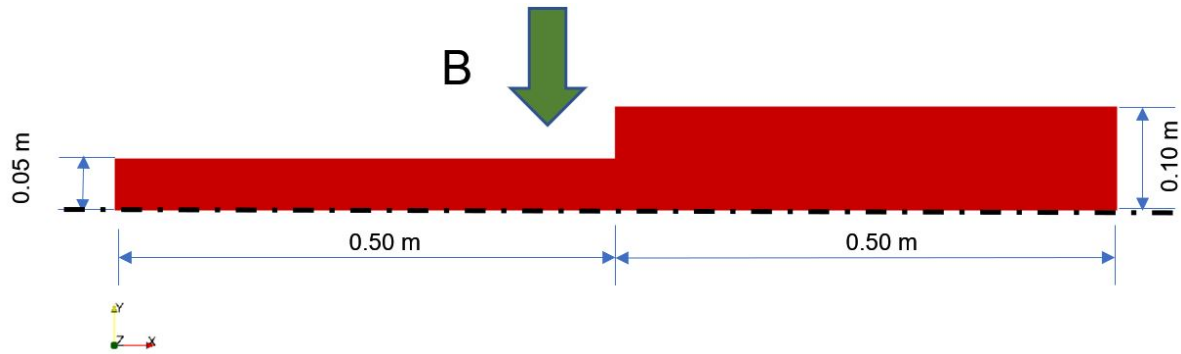


Figure 8. Dimensions in x-y plane

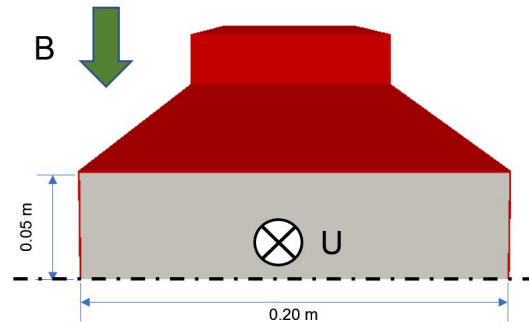


Figure 9. Dimensions in the plane perpendicular to the flow velocity

The characteristic length of the case, constant all along the domain, is $L_s = 0.10$ m, half of the width in the direction perpendicular to the magnetic field and perpendicular to the velocity field. The dimensionless numbers that characterize the flow are the Hartmann number ($Ha = BL_s \sqrt{\sigma/\mu}$), the Reynolds number ($Re = \rho \bar{U} L_s / \mu$), and the wall conductance ratio ($c_w = \sigma_w t_w / \sigma L_s$). B stands for the magnetic field intensity, σ is the electric conductivity of the fluid, μ is the dynamic viscosity, ρ is the fluid density, \bar{U} is the mean velocity at the narrow part of the channel, σ_w is the electric conductivity of the wall, and t_w is the wall width. Note that the characteristic length to define this case (L_s) is not the same as the usual, L_h , half width in the direction of the magnetic field.

The EUROFER electric conductivity is $8.33 \cdot 10^5$ S/m and has been obtained from reference [30]. This corresponds to $c_w = 0.01$, and since this study will scan different values of c_w , the variable parameter will be the wall electric conductivity, while the wall thickness will be kept constant.

The velocity field has the non-slip boundary condition in contact with the inner face of the surrounding walls and has a zero gradient boundary condition in inlet and outlet patches.

A fixed pressure gradient $\partial p/\partial x$ has been set at the inlet patch to keep the desired inlet flow rate while a fixed value of zero has been forced at the outlet patch.

The electric potential boundary conditions on the outer walls and in the inlet and outlet regions are of zero gradient. The electric potential at the solid-liquid interface is the same in both materials. The electric current can pass from the solid wall to the fluid and vice versa.

In order to reduce the computation time, the fully developed result for the inlet straight section and for the outlet straight section have been calculated and mapped into the full case, leaving only the 3D MHD effect to be solved.

The meshing criteria has been similar to previous studies from our group [31], keeping 5 cells for Hartmann boundary layer ($2L_h/Ha$ next to the walls perpendicular to the magnetic field) and 19 for side boundary layer ($3L_h/\sqrt{Ha}$ next to the walls parallel to the magnetic field). Note that L_h corresponds to the half width of the channel in the direction of the magnetic field, whereas L_s , the characteristic length for the dimensionless variables, is half width in the perpendicular direction. In terms of mesh refinement in the boundary layers, using L_h is conservative compared to using L_s . The rest of the bulk and wall cells are configured by a smooth cell-to-cell grading lower than 10% in any case.

The simulations were run in the *Marconi HPC* in Italy. The availability to use such tool allowed to increase the Hartmann number of the simulations (Ha determines the required mesh refinement). The automation of the cases run included the manual selection of the domain regions to be distributed among the available processors, and the use of the SLURM workload manager. The number of processors used in each case was 48.

The selected set of cases was the combination of three dimensionless numbers ($Re=250, 500$ and 750 , $Ha=250, 500$ and 750 and $c_w=0.001, 0.01$ and 0.1) to generate $3^3 = 27$ cases for the contraction and 27 cases for the expansion. Mesh size for cases with $Ha=250$ is $\sim 4250k$ cells, for $Ha=500$ is $\sim 7750k$ and for $Ha=750$ is $\sim 8500k$. For cases with $Ha=750$ only 4 cells have been placed in the Hartmann boundary layer and 15 cells in the side boundary layer.

Each case, run on 48 processors, took between one and two weeks to complete, depending on the number of cells in the mesh.

3.3. Results

The results of the simulations for the contraction case are shown in Tables 2 and 3. The results of the expansion case are shown in Tables 4 and 5. The cases have been ordered by the c_w and N , from lower to higher. N stands for the Stuart number (interaction parameter). The detail of the information contained in the tables is commented here

whereas the analysis of the results is discussed in the next section.

Table 2. Results for the contraction liquid metal MHD flows. Pressure drops

MHD contraction pressure drops results								
Ha	Re	c_w	N	$\partial p/\partial x_{out}$ (Pa/m)	$\partial p/\partial x_{in}$ (Pa/m)	Total Pres- sure Drop (Pa)	ξ_P	k_P
250	750	0.001	83	0.112	0.028	0.15	12.54	0.15
250	500	0.001	125	0.075	0.019	0.10	19.29	0.15
250	250	0.001	250	0.037	0.009	0.05	35.07	0.14
500	750	0.001	333	0.264	0.066	0.39	34.17	0.10
500	500	0.001	500	0.176	0.044	0.28	57.91	0.12
750	750	0.001	750	0.457	0.114	0.84	85.92	0.11
500	250	0.001	1000	0.088	0.022	0.13	103.33	0.10
750	500	0.001	1125	0.305	0.076	0.53	116.69	0.10
750	250	0.001	2250	0.152	0.038	0.25	220.31	0.10
250	750	0.01	83	0.298	0.074	0.28	14.14	0.17
250	500	0.01	125	0.198	0.050	0.18	20.10	0.16
250	250	0.01	250	0.099	0.025	0.09	36.15	0.14
500	750	0.01	333	0.998	0.248	0.88	40.18	0.12
500	500	0.01	500	0.665	0.165	0.59	60.93	0.12
750	750	0.01	750	2.098	0.519	1.80	76.37	0.10
500	250	0.01	1000	0.333	0.083	0.29	111.19	0.11
750	500	0.01	1125	1.399	0.346	1.24	128.16	0.11
750	250	0.01	2250	0.699	0.173	0.60	229.94	0.10
250	750	0.1	83	1.744	0.442	1.20	15.81	0.19
250	500	0.1	125	1.163	0.294	0.79	22.55	0.18
250	250	0.1	250	0.581	0.147	0.40	42.90	0.17
500	750	0.1	333	6.715	1.682	4.40	30.31	0.09
500	500	0.1	500	4.477	1.121	2.99	65.68	0.13
750	750	0.1	750	14.893	3.706	9.96	102.07	0.14
500	250	0.1	1000	2.238	0.561	1.51	151.37	0.15
750	500	0.1	1125	9.928	2.471	6.58	131.83	0.12
750	250	0.1	2250	4.964	1.235	3.32	310.16	0.14

Tables 2 and 4 summarize the results associated with the pressure drop approach. There, one can find the pressure drop per meter $\partial p/\partial x$ in (Pa/m) for the inlet and outlet fully developed straight channels under the conditions of Ha , Re and c_w . The total pressure drop in Pa of the whole domain can be found as well as the ξ_P and k_P . Note that in order to compute the pressure drop of the singularity alone, Δp_{3D} , the pressure drop in the inlet and outlet straight channels must be withdrawn from the total pressure drop (Δp_{total}). Since they are 0.5 m long, $\Delta p_{3D} = \Delta p_{total} - \partial p/\partial x_{in} \cdot 0.5 - \partial p/\partial x_{out} \cdot 0.5$. Using Re , μ , ρ and L_s one can find \bar{U} . Following Eq. 18, ξ_p can be found.

Table 3. Results for the contraction liquid metal MHD flows. Head losses

MHD contraction head losses results										
Ha	Re	c_w	N	Power Loss (J/s)	Total head Loss (Pa)	Sing. head Loss (Pa)	α_{out}	α_{in}	ξ_H	k_H
250	750	0.001	83	1.69E-06	0.15	0.08	1.06	1.05	11.83	0.14
250	500	0.001	125	7.70E-07	0.10	0.05	1.06	1.05	18.52	0.15
250	250	0.001	250	1.85E-07	0.05	0.02	1.06	1.05	34.28	0.14
500	750	0.001	333	4.41E-06	0.38	0.22	1.04	1.03	33.42	0.10
500	500	0.001	500	2.11E-06	0.27	0.16	1.04	1.03	57.12	0.11
750	750	0.001	750	9.68E-06	0.84	0.55	1.03	1.02	85.17	0.11
500	250	0.001	1000	4.96E-07	0.13	0.07	1.04	1.03	102.55	0.10
750	500	0.001	1125	4.04E-06	0.52	0.33	1.03	1.02	115.97	0.10
750	250	0.001	2250	9.76E-07	0.25	0.16	1.03	1.02	219.54	0.10
250	750	0.01	83	3.15E-06	0.27	0.09	1.05	1.04	13.37	0.16
250	500	0.01	125	1.38E-06	0.18	0.06	1.05	1.04	19.32	0.15
250	250	0.01	250	3.37E-07	0.09	0.03	1.05	1.04	35.37	0.14
500	750	0.01	333	1.02E-05	0.88	0.26	1.11	1.06	39.52	0.12
500	500	0.01	500	4.53E-06	0.59	0.17	1.09	1.06	60.16	0.12
750	750	0.01	750	2.08E-05	1.80	0.49	1.15	1.10	75.55	0.10
500	250	0.01	1000	1.11E-06	0.29	0.08	1.09	1.06	110.42	0.11
750	500	0.01	1125	9.54E-06	1.24	0.37	1.11	1.11	127.25	0.11
750	250	0.01	2250	2.31E-06	0.60	0.17	1.14	1.10	229.09	0.10
250	750	0.1	83	1.37E-05	1.19	0.10	1.65	1.30	14.92	0.18
250	500	0.1	125	6.09E-06	0.79	0.06	1.65	1.30	21.66	0.17
250	250	0.1	250	1.52E-06	0.39	0.03	1.65	1.30	42.01	0.17
500	750	0.1	333	5.07E-05	4.39	0.19	2.79	1.62	29.27	0.09
500	500	0.1	500	2.30E-05	2.99	0.19	2.52	1.62	64.55	0.13
750	750	0.1	750	1.15E-04	9.95	0.65	3.53	1.95	100.92	0.13
500	250	0.1	1000	5.81E-06	1.51	0.11	2.46	1.62	150.37	0.15
750	500	0.1	1125	5.07E-05	6.58	0.38	4.00	1.95	131.71	0.12
750	250	0.1	2250	1.28E-05	3.32	0.22	3.38	1.95	308.99	0.14

The "p" subscript has been added to differentiate the pressure drop results from those corresponding to the head losses calculation. k_p , similarly, is $\xi_p = k_p \cdot N$.

Tables 3 and 5 summarize the results of the head loss approach. They display the mechanical power loss (J/s) in the whole domain (as computed in Eq. 9), the total head loss (Eq. 7) and the singularity head loss, $h_{L \text{ singularity}}$ (Eq. 10). The kinetic energy correction factors, α , for the inlet and outlet fully developed regions are also shown, along with the singular head loss coefficient, $\xi_H = h_{L \text{ sing.}} / (\rho \bar{U}^2 / 2)$ and $k_H = \xi_H \cdot N$. The "H" subscript has been used for the head loss results.

Table 4. Results for the expansion liquid metal MHD flows. Pressure drops

MHD expansion pressure drops results								
Ha	Re	c_w	N	$\partial p/\partial x_{out}$ (Pa/m)	$\partial p/\partial x_{in}$ (Pa/m)	Total Pres- sure Drop (Pa)	ξ_P	k_P
250	750	0.001	83	0.112	0.028	0.11	6.07	0.07
250	500	0.001	125	0.075	0.019	0.10	17.45	0.14
250	250	0.001	250	0.037	0.009	0.05	34.82	0.14
500	750	0.001	333	0.264	0.066	0.85	105.31	0.32
500	500	0.001	500	0.176	0.044	0.29	63.61	0.13
750	750	0.001	750	0.457	0.114	0.68	60.50	0.08
500	250	0.001	1000	0.088	0.022	0.14	117.72	0.12
750	500	0.001	1125	0.305	0.076	0.43	83.38	0.07
750	250	0.001	2250	0.152	0.038	0.18	111.66	0.05
250	750	0.01	83	0.298	0.074	0.31	18.69	0.22
250	500	0.01	125	0.198	0.050	0.18	18.41	0.15
250	250	0.01	250	0.099	0.025	0.09	34.42	0.14
500	750	0.01	333	0.998	0.248	0.83	32.11	0.10
500	500	0.01	500	0.665	0.165	0.57	53.74	0.11
750	750	0.01	750	2.098	0.519	1.78	72.26	0.10
500	250	0.01	1000	0.333	0.083	0.27	87.63	0.09
750	500	0.01	1125	1.399	0.346	0.89	7.17	0.01
750	250	0.01	2250	0.699	0.173	0.44	5.80	0.00
250	750	0.1	83	1.744	0.442	1.18	14.04	0.17
250	500	0.1	125	1.163	0.294	0.79	20.83	0.17
250	250	0.1	250	0.581	0.147	0.39	40.34	0.16
500	750	0.1	333	6.715	1.682	4.51	48.14	0.14
500	500	0.1	500	4.477	1.121	2.93	45.07	0.09
750	750	0.1	750	14.893	3.706	9.95	100.77	0.13
500	250	0.1	1000	2.238	0.561	1.51	152.92	0.15
750	500	0.1	1125	9.928	2.471	7.01	282.25	0.25
750	250	0.1	2250	4.964	1.235	3.63	736.78	0.33

4. Discussion

In liquid metal MHD flows through insulated channels, or in low c_w channels, the flow profile is mostly flat. Although the flow regime is laminar, this implies an α coefficient very close to 1, similar to the hydrodynamic turbulent flows. This can be observed in those cases with $c_w = 0.001$, even at the highest N . It can also be observed that, for high wall conductivity ratio ($c_w = 0.1$), the α coefficient reaches higher values.

The modification of the α coefficient in an expansion/contraction of a liquid metal MHD flow was anticipated before developing this study. The original thought was that

Table 5. Results for the expansion liquid metal MHD flows. Head losses

MHD expansion head losses results										
Ha	Re	c_w	N	Power Loss (J/s)	Total head Loss (Pa)	Sing. head Loss (Pa)	α_{out}	α_{in}	ξ_H	k_H
250	750	0.001	83	1.32E-06	0.11	0.04	1.05	1.06	6.83	0.08
250	500	0.001	125	7.63E-07	0.10	0.05	1.05	1.06	18.23	0.15
250	250	0.001	250	1.88E-07	0.05	0.03	1.05	1.06	35.58	0.14
500	750	0.001	333	9.84E-06	0.85	0.69	1.03	1.03	106.00	0.32
500	500	0.001	500	2.28E-06	0.30	0.19	1.03	1.04	64.40	0.13
750	750	0.001	750	7.89E-06	0.68	0.40	1.02	1.03	61.25	0.08
500	250	0.001	1000	5.40E-07	0.14	0.09	1.03	1.04	118.50	0.12
750	500	0.001	1125	3.33E-06	0.43	0.24	1.02	1.03	84.09	0.07
750	250	0.001	2250	6.79E-07	0.18	0.08	1.02	1.04	112.49	0.05
250	750	0.01	83	3.60E-06	0.31	0.13	1.04	1.05	19.45	0.23
250	500	0.01	125	1.38E-06	0.18	0.06	1.04	1.06	19.14	0.15
250	250	0.01	250	3.36E-07	0.09	0.03	1.04	1.05	35.19	0.14
500	750	0.01	333	9.67E-06	0.84	0.21	1.06	1.06	33.06	0.10
500	500	0.01	500	4.41E-06	0.57	0.16	1.06	1.07	54.57	0.11
750	750	0.01	750	2.06E-05	1.78	0.47	1.10	1.17	72.98	0.10
500	250	0.01	1000	1.04E-06	0.27	0.06	1.06	1.08	88.40	0.09
750	500	0.01	1125	6.89E-06	0.90	0.02	1.10	1.13	7.89	0.01
750	250	0.01	2250	1.70E-06	0.44	0.00	1.10	1.13	6.53	0.00
250	750	0.1	83	1.37E-05	1.19	0.10	1.30	1.66	14.92	0.18
250	500	0.1	125	6.09E-06	0.79	0.06	1.30	1.65	21.72	0.17
250	250	0.1	250	1.52E-06	0.39	0.03	1.30	1.65	41.24	0.16
500	750	0.1	333	5.22E-05	4.52	0.32	1.62	2.47	49.23	0.15
500	500	0.1	500	2.26E-05	2.93	0.13	1.62	2.68	45.07	0.09
750	750	0.1	750	1.15E-04	9.96	0.66	1.95	3.50	101.92	0.14
500	250	0.1	1000	5.82E-06	1.51	0.11	1.62	2.45	153.93	0.15
750	500	0.1	1125	5.39E-05	7.00	0.80	1.95	3.54	278.08	0.25
750	250	0.1	2250	1.40E-05	3.63	0.53	1.94	3.39	730.39	0.32

if the expansion/contraction occurs in the direction of the magnetic field, the Hartmann number at the inlet and at the outlet are different because of the different characteristic length. Note that the Hartmann number in fully developed flows should be calculated using L_h as characteristic length. When the channel expands in the direction of the magnetic field, L_h doubles, and the Hartmann number too; the wall conductivity ratio, however, halves. If the walls are conducting, the magnitude of the jets appearing in the vicinity of the side walls and, therefore, the flow distribution (the α coefficient), will change from inlet to outlet. This has been confirmed in the simulations.

The objective of this study was to understand the implications of this effect (the modification of the α coefficient) in the pressure drop associated to such singularities.

The idea was to quantify the difference between the pressure drop and the head loss.

When the liquid metal flow encounters the singularity, either a contraction or an expansion, the Lorentz forces are high enough to produce an actual pressure drop in all the cases simulated. This is an important difference compared to the results obtained for the hydrodynamic analysis, where pressure can increase in expansions. The importance of such pressure drop in the head loss varies from case to case. Some examples can be seen in Figure 10.

Looking at those cases with low c_w , it can be seen that the higher the N value, the higher the contribution of pressure drop to the head loss. Furthermore, in all cases of low c_w , the rationale made for hydrodynamic flows in a contraction (where the kinetic energy increases) and in an expansion (where kinetic energy drops), is still valid.

Regarding the results for high c_w , shown in Figure 11 the same phenomena occurs, where the higher the value of N , the higher the contribution of the pressure drop on the head loss. Since the MHD pressure drop scales with N , and the kinetic energy change does not, this result could have been anticipated. The surprising phenomena observed for high c_w cases ($c_w = 0.1$ cases) is that the rationale encountered in hydrodynamic flows, where the kinetic energy increases in contractions and decreases in expansions, does not apply for high values of N , such as $N = 750$, for example. In the contraction case, there is a kinetic energy drop of 3% of the head loss magnitude, and the same anomaly is encountered in the expansion case, where the kinetic energy increases. Recalling Eq. 15, it is easy to observe that, since the change in mean velocity is associated to the change in geometry, the only parameter that can alter the kinetic energy balance is the α coefficient. Indeed, in Tables 3 and 5 it can be observed that for high c_w and high N there is an important modification in the kinetic energy correction factor α at inlet and outlet. This result is counter-intuitive and highlights the importance of the flow velocity distribution. The velocity distribution for two relevant cases is shown in Figure 12.

From the data obtained for the k_p values, it can be seen that most cases present results lower than 0.25, which is the lower limit of the range found experimentally (see comments after Eq. 18).

Although in this work the only studied singularities have been sudden contractions and expansions, the momentum transfer approach can also be applied to cases with multiple inlets and outlets, e.g. manifolds. The method requires to compute the mechanical energy at each of the boundaries where there is inflow or outflow.

To properly apply the method proposed in this work, it is crucial that the 3D domain calculated with the CFD code contains both the departure from (at the inlet) and the reestablishment of (at the outlet) the fully developed flow regime. When the procedure is applied, it yields the energy loss at the manifold singularity.

Considering the relevant parameters in fusion reactor blankets, the magnitude of the N values is high enough in all blanket types 'Helium Cooled Lead-Lithium (HCLL), WCLL, DCLL' to rely in the pressure drop analysis, and neglect the influence of the kinetic energy change in expansions and contractions. However, the calculation

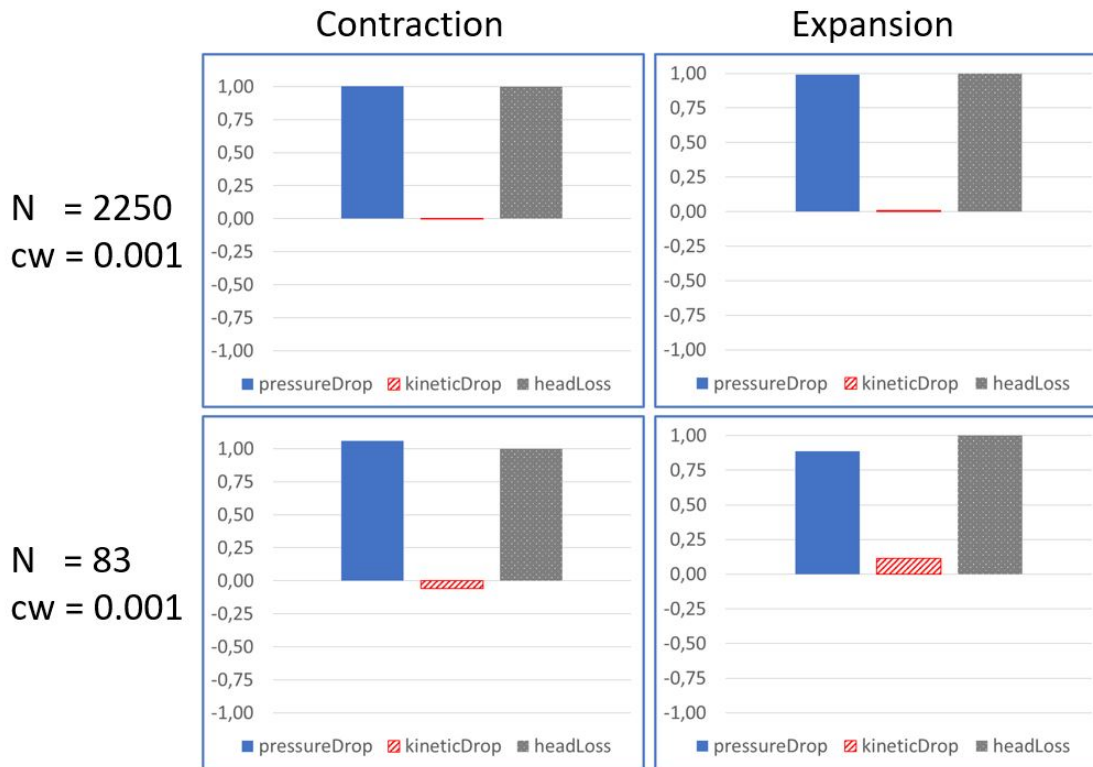


Figure 10. Pressure drop and kinetic energy drop contribution to the singularity head loss in contractions and expansions for selected cases with $c_w = 0.001$

procedure explained in this work is recommended for the head losses analysis in manifolds that contain multiple inlets and/or outlets.

5. Conclusions

The aim of the present work was to fully understand the relationship between the pressure drop and the head losses of a geometric singularity.

As shown in the first part of the article, when an incompressible laminar flow encounters a sudden expansion, it transforms part of the kinetic energy into pressure. To assess the influence of such a singularity on the entire fluid system, the head loss provides more relevant information than the pressure drop.

In order to analyse the head loss phenomenon, series of hundreds of CFD simulations have been executed for the hydrodynamic pipe cases. In the first part of the article the importance of the kinetic energy correction factor α in Bernoulli's system balance has also been outlined. The α factor in the kinetic energy term carries the information derived from the addition of the momentum crossing all the faces of boundary cells at a given boundary of the system.

In the second part, the methodology outlined and validated with hydrodynamic flows has been applied to liquid metal MHD flows in rectangular contractions and expansions.

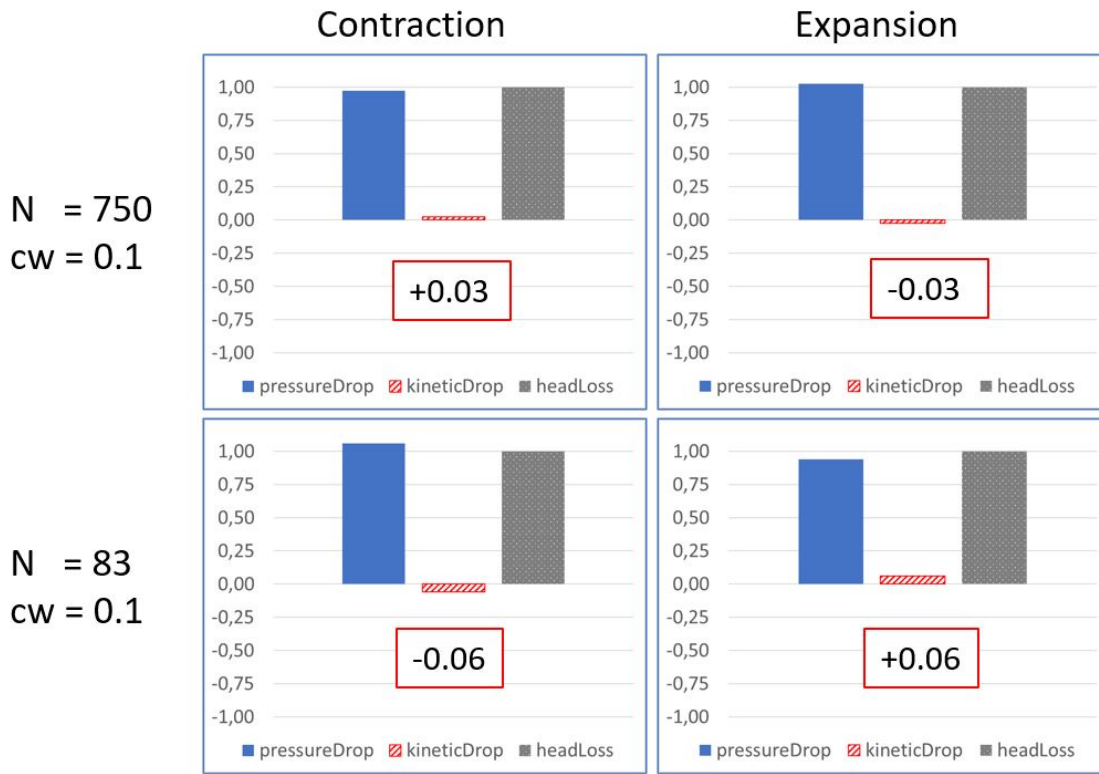


Figure 11. Pressure drop and kinetic energy drop contribution to the singularity head loss in contractions and expansions for selected cases with $c_w = 0.1$

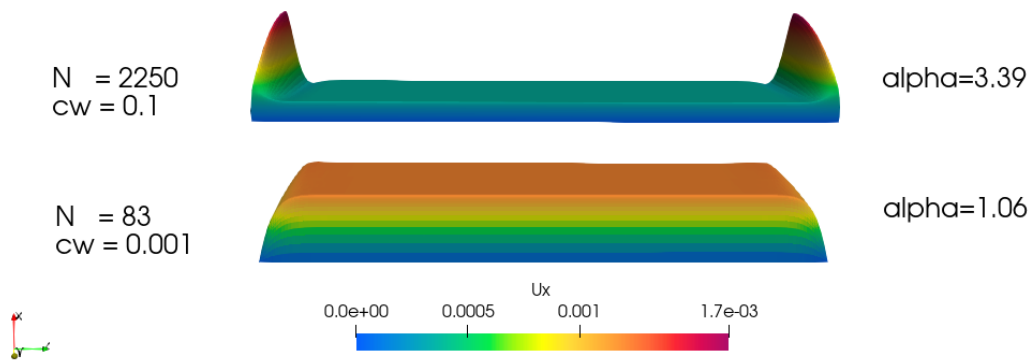


Figure 12. Velocity distribution profile (x axis) over half cross-sectional plane of the narrow channel and associated kinetic energy correction factor (α) for cases $N=83$ $c_w=0.001$, and for $N=2250$ $c_w=0.1$. Note the Reynolds number is different in both cases. The velocity is in units of [m/s]

The first conclusion of the application of such methodology is that the use of the pressure drop instead of head loss for liquid metal MHD flows in contractions and expansions carries a very small error. The deviation for the lowest Stuart number

(interaction parameter), N , considered in this study ($N = 83$ and $c_w = 0.001$), is less than 1%; the magnitude of the error decreases as N increases.

There have been, however, some interesting conclusions to outline regarding the relationship between head loss, pressure drop, and the change in kinetic energy in the domain. In those cases with high interaction parameter, N , and high wall conductance ratios, c_w , the velocity distribution changes and the fluid can gain kinetic energy, even in an expansion, where the mean velocity decreases. The parameter that indicates the distribution of such flow is the kinetic energy correction factor, that is very large in such situations thanks to the large jets generated at the outlet.

An analogous situation occurs in the cases of sudden contraction. The mean velocity increases, therefore, the kinetic energy increases, provoking a higher pressure drop, that in this case is higher than the domain head loss. For the same ranges of high N and high c_w , the impact of the flow distribution in the results is such that the pressure drop becomes smaller than the head loss, just like in a hydrodynamic expansion.

The procedure described in this article can also be applied to a domain with several inlets or outlets. The robustness of the method has been proved and can be used any time a component head loss needs to be evaluated (e.g., in order to use CFD results for system code modelling).

Acknowledgments

This work has been carried out within the framework of the EUROfusion Consortium and has received funding from the Euratom research and training programme 2014-2018 and 2019-2020 under grant agreement No. 633053. The views and opinions expressed herein do not necessarily reflect those of the European Commission. Authors also thank EUROfusion for the allocation of HPC capacity on Marconi-Fusion and Marconi100. Authors thank as well the contribution of Associació/Col·legi d'Enginyers Industrials de Catalunya with Fundació Caixa d'Enginyers' financial support.

Bibliography

- [1] U Müller and L Bühler. *Magnetofluidynamics in Channels and Containers*. 2001.
- [2] S Malang, H Deckers, U Fischer, H Reiser, and K Rust. Self-cooled blanket concepts using Pb-17Li as liquid breeder and coolant. *Fusion Engineering and Design*, 14:373–399, 1991.
- [3] S. Molokov. Liquid metal flows in insulating elements of self-cooled blankets. *Fusion Engineering and Design*, 27(C):642–649, 1995.
- [4] C. Mistrangelo and L. Bühler. Numerical investigation of liquid metal flows in rectangular sudden expansions. *Fusion Engineering and Design*, 82(15-24):2176–2182, 2007.
- [5] L. Bühler, S. Horanyi, and E. Arbogast. Experimental investigation of liquid-metal flows through a sudden expansion at fusion-relevant Hartmann numbers. *Fusion Engineering and Design*, 82(15-24):2239–2245, 2007.
- [6] Sergey Smolentsev, Tyler Rhodes, Gautam Pulugundla, Cyril Courtessole, Mohamed Abdou, Siegfried Malang, Mark Tillack, and Chuck Kessel. MHD thermohydraulics analysis and

- supporting R&D for DCLL blanket in the FNSF. *Fusion Engineering and Design*, 135:314–323, 2018. Special Issue: FESS-FNSF Study.
- [7] Alessandro Tassone, Gianfranco Caruso, and Alessandro Del. Influence of PbLi hydraulic path and integration layout on MHD pressure losses. *Fusion Engineering and Design*, 155(July 2019):111517, 2020.
- [8] Sergey Smolentsev. Physical Background, Computations and Practical Issues of the Magnetohydrodynamic Pressure Drop in a Fusion Liquid Metal Blanket. *Fluids*, 6(3), 2021.
- [9] Daniel Suarez, Elisabet Mas de les Valls, and Lluís Batet. Mhd assessment in dcll back manifold. part i, uncoupled flows. *Eurofusion Internal Report: WPBB-DEL-BB-5.2.2-T002-D003*, 2018.
- [10] Andrei Khodak, Peter Titus, Thomas Brown, and Jonathan Klabacha. Numerical model of dual-coolant lead – lithium (DCLL) blanket. *Fusion Engineering and Design*, 137(November 2016):124–129, 2018.
- [11] Gianni Astarita and Guido Greco. Excess pressure drop in laminar flow through sudden contraction. *Newtonian Liquids*, 7(1), 1968.
- [12] S E Kaye and S L Rosen. The Dependence of Laminar Entrance Loss Coefficients on Contraction Ratio for Newtonian Fluids. *AIChE*, 1(5):1269–1270, 1971.
- [13] I E Idelchik. *Handbook of Hydraulic Resistance*. begel house, inc., 4th edition, 2008.
- [14] E.F. Brater, H.W. King, J.E. Lindell, and C.Y. Wei. *Handbook of Hydraulic*. McGraw-Hill, Inc., 7th edition, 1996.
- [15] DS Miller. *Internal flow systems*. BHRA The Fluid Engineering Center, 1978.
- [16] CRANE CO. *Flow of Fluids*. 1982.
- [17] Y Cengel and J Cimbala. *Essentials of Fluid Mechanics: Fundamentals and Applications*. 2008.
- [18] Yan Jin. Second-law analysis: A powerful tool for analyzing Computational Fluid Dynamics (CFD) results. *Entropy*, 19(12):19–21, 2017.
- [19] Bastian Schmandt, Vasudevan Iyer, and Heinz Herwig. Determination of head change coefficients for dividing and combining junctions: A method based on the second law of thermodynamics. *Chemical Engineering Science*, 111:191–202, 2014.
- [20] N.D. Sylvester and S L Rosen. Laminar Flow in the Entrance Region of a Cylindrical Tube: Part I. Newtonian Fluids. *AIChE*, (15):964–966, 1970.
- [21] F Durst and T Loy. Investigations of laminar flow in a pipe with sudden contraction of cross sectional area. *Computers & Fluids*, 13(1):15–36, 1985.
- [22] P. R. Bullen, D. J. Cheeseman, L. A. Hussain, and A. E. Ruffell. The determination of pipe contraction pressure loss coefficients for incompressible turbulent flow. *International Journal of Heat and Fluid Flow*, 8(2):111–118, 1987.
- [23] Ludicelo, F. Flow in pipes with sudden contraction. https://www.kbwiki.ercoftac.org/w/index.php?title=Abstr:Flow_in_pipes_with_sudden_contraction, 2017. ERCOFTAC. Accessed: 2020-12-12.
- [24] S. Patankar. *Numerical Heat Transfer and Fluid Flow*. McGraw-Hill Book Company, 1980.
- [25] H. G. Weller, G. Tabor, H. Jasak, and C. Fureby. A tensorial approach to computational continuum mechanics using object-oriented techniques. *Computers in Physics*, 12(6):620, 1998.
- [26] Ismail Celik, U Ghia, P.J. Roache, Chris Freitas, H Coloman, and Peter Raad. Procedure of estimation and reporting of uncertainty due to discretization in cfd applications. *J. Fluids Eng.*, 130, 2008.
- [27] Elisabet Mas de les Valls. *Development of a simulation tool for MHD flows under nuclear fusion conditions*. PhD dissertation, Dept. of Physics and Nuclear Engineering, Universitat Politècnica de Catalunya, 2011.
- [28] Ming-Jiu Ni, Ramakanth Munipalli, Neil B Morley, Peter Huang, and Mohamed A Abdou. A current density conservative scheme for incompressible MHD flows at a low magnetic Reynolds number . Part I : On a rectangular collocated grid system. *Journal of Computational Physics*, 227, 2007.
- [29] Elisabet Mas de les Valls, L.A. Sedano, L. Batet, I. Ricapito, A. Aiello, O. Gastaldi, and F. Gabriel. Lead–lithium eutectic material database for nuclear fusion technology. *Journal of Nuclear*

Materials, 376, 2008.

- [30] F. Ugorri, S. Smolentsev, I. Fernández-Berqueruelo, D. Rapisarda, I. Palermo, and A. Ibarra. Magnetohydrodynamic and thermal analysis of PbLi flows in poloidal channels with flow channel insert for the EU-DCLL blanket. *Nuclear Fusion*, 58, 2018.
- [31] Dionisio Di Giulio, Daniel Suarez, Lluís Batet, Elisabet Mas de les Valls, and Laura Savoldi. Analysis of flow channel insert deformations influence on the liquid metal flow in dcll blanket channels. *Fusion Engineering and Design*, 157:111639, 2020.